Rotor Speed-Based Bearing Fault Diagnosis (RSB-BFD) Under Variable Speed and Constant Load

Moussa Hamadache, *Student Member, IEEE*, Dongik Lee, *Member, IEEE*, and Kalyana C. Veluvolu, *Senior Member, IEEE*

***Abstract*—This paper addresses the application of rotor speed signal for the detection and diagnosis of ball bearing faults in rotating electrical machines. Many existing techniques for bearing fault diagnosis (BFD) rely on vibration signals or current signals. However, vibration- or current-based BFD techniques suffer from various challenges that must be addressed. As an alternative, this paper takes the initial step of investigating the efficiency of rotor speed monitoring for BFD. The bearing failure modes are reviewed and their effects on the rotor speed signal are described. Based on this analysis, a novel BFD technique, the rotor speed-based BFD (RSB-BFD) method under variable speed and constant load conditions, is proposed to provide a benefit in terms of cost and simplicity. The proposed RSB-BFD method exploits the absolute value-based principal component analysis (PCA), which improves the performance of classical PCA by using the absolute value of weights and the sum square error. The performance and effectiveness of the RSB-BFD method is demonstrated using an experimental setup with a set of realistic bearing faults in the outer race, inner race, and balls.**

***Index Terms*—Bearing fault diagnosis (BFD), principal component analysis (PCA), rotor speed, sum square error, variable speed.**

I. Introduction

FAULT DIAGNOSIS techniques are becoming more important as more engineering processes are automated while the manpower needed to operate and supervise processes is reduced. Because rotating electrical machines (REMs) are at the heart of most engineering processes and are designed for tighter margins, there is a growing need for fault diagnosis for the sake of reliability. Different faults may occur in a REM, which can be classified as stator faults, rotor faults, static and dynamic eccentricities, and bearing faults [1]. Based on an IEEE motor reliability study for large motors above 200 hp [2], bearing faults are the most significant single cause of motor failure (41%), followed by stator faults (37%) and rotor faults (10%). In fact, rolling bearings are used not only in motors but also in almost every industrial process that involves rotating and reciprocating machinery [3].

Existing techniques for bearing fault diagnosis (BFD) require more data acquisition equipment and additional measurements, such as vibrations, temperature, acoustic emissions, and stator current monitoring [4]. In particular, recent surveys [5]–[10] indicate a clear tendency toward the vibration monitoring of REMs. However, despite the fact that vibration-based BFD techniques have been successfully applied and are increasingly deployed in industry [11]–[14], challenges still exist that must be addressed. Vibration sensors, such as accelerometers, are mounted on the surface of system components, which are installed deep inside machinery and are difficult to access during real-time operation. The sensors and equipment are also inevitably subject to failure, which could cause additional problems with system reliability and result in additional operating and maintenance costs [15]. Moreover, in the case of varying speeds, the vibration signal from the bearings is affected by operation, which makes diagnosis difficult. These difficulties are due to the variation of diagnostic features caused primarily by speed variations, low energy of sought features, and high noise levels.

As an alternative, several researchers [15]–[17] have proposed stator current-based techniques under the assumption that the machine operates at a constant supply frequency at steady state. Unfortunately, this assumption may be unrealistic in an actual system. Stator current-based approaches also suffer from the fact that stator current signals can be used only if there is a large failure. Note that the detection of an extremely early incipient fault is essential in BFD because a minor bearing fault can rapidly become a serious failure.

To overcome the challenges with existing BFD techniques based on vibration or stator current signals, this paper explores the application of a rotor speed signal to the detection and diagnosis of ball bearing faults (BBFs) in REMs. The proposed rotor speed-based BFD (RSB-BFD) method assumes variable rotor speed conditions and only uses rotor speed measurements. Since speed signals are reliable and easily accessible as compared to vibration signals, this approach can be beneficial in terms of low cost, simplicity, and reliability. However, it is

Manuscript received August 9, 2014; revised September 19, 2014 and January 13, 2015; accepted February 12, 2015. Date of publication March 25, 2015; date of current version September 9, 2015. This work was supported by the International Research and Development Program of the National Research Foundation of Korea (NRF) funded by the Ministry of Science, Information, and Communications Technologies (ICT) and Future Planning of Korea under Grant NRF-2012K1A3A7A03057508.

The authors are with the School of Electronics Engineering, Kyungpook National University, Daegu 702-701, Korea (e-mail: dilee@ee.knu.ac.kr).

Color versions of one or more of the figures in this paper are available online at http://ieeexplore.ieee.org.

Digital Object Identifier 10.1109/TIE.2015.2416673

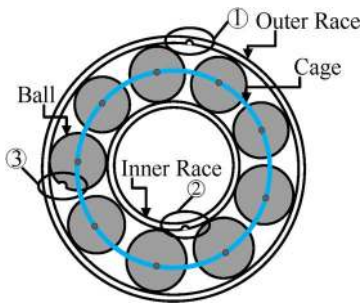

Fig. 1. Ball bearing geometry and the possible defects.

important to note that the frequency domain analysis of a speed signal shows no significant distinction between different bearing faults, which is the primary reason why rotor speed-based BFD has not been used. To solve this problem, we propose the absolute value-based principal component analysis (PCA) (AVPCA), in which the classical PCA, a well-known feature extraction method, is modified to calculate the PCA bases using the absolute value of weights and the sum square error distances.

This paper is organized as follows. In Section II, an analysis of rotor speed signals under bearing faults is presented. Section III introduces the AVPCA, which is used for the proposed RSB-BFD method. In Section IV, the proposed AVPCA-based algorithm for bearing fault detection and diagnosis is presented, where experimental results are shown in Section V. Finally, discussion and conclusion are presented in Section VI.

II. Rotor Speed Signal Under Bearing Faults

A. Bearing Fault Types

Based on the fault classification in [17], bearing faults can be categorized into two types: 1) single-point faults, which are defined as a visible single fault; and 2) generalized roughness, which refers to a damaged bearing. A single-point fault produces a characteristic fault frequency that depends on the surface of the bearing that contains the fault. Because most rotating machines use rolling-element bearings that consist of an outer race and an inner race, single-point faults in a bearing considered in this study include the following: 1) outer-race fault (ORF); 2) inner-race fault (IRF); and 3) ball bearing fault (BBF), as shown in Fig. 1. The bearing fault-free case is denoted by BFF.

A bearing fault introduces specific frequency components that depart from the normal distribution, which subsequently increases the kurtosis value. Fault-related torque oscillations at particular frequencies are often related to the shaft speed. The characteristic bearing fault frequency f_c in different bearing faults is given by the following relationships [11]:

$$f_c = \begin{cases} f_{out} = \frac{N_b}{2} f_r \left(1 - \frac{d_b \cos\beta}{d_p}\right) & \text{for ORF} \\ f_{in} = \frac{N_b}{2} f_r \left(1 + \frac{d_b \cos\beta}{d_p}\right) & \text{for IRF} \\ f_{ball} = \frac{d_p}{d_b} f_r \left(1 - \left(\frac{d_b \cos\beta}{d_p}\right)^2\right) & \text{for BBF} \end{cases} \quad (1)$$

where f_{out} is the ORF frequency, f_{in} is the IRF frequency, f_{ball} is the ball fault frequency, d_b is the ball diameter, d_P is the pitch ball diameter, N_b is the number of balls, β is the ball contact angle (with the races), and f_r is the mechanical rotor frequency.

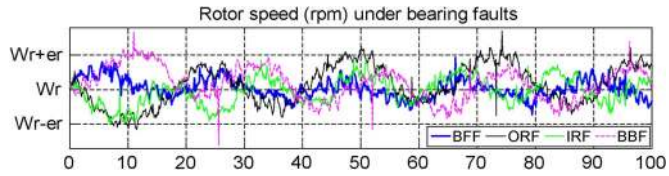

Fig. 2. Measurements of the rotor speed under constant load for different bearing faults with $T_s = 58.61$ μs, $w_r = 2500$ r/min, and $e_r = 10^{-4}$.

B. Effect of Bearing Faults on Rotor Speed Signal

In this section, additional details on the effect of a bearing fault on the rotor speed will be introduced, which account for fault-related variable speed. The method used to study the influence of the bearing fault on the rotor speed is related to the magnetomotive force. To the authors' knowledge, this method has not yet been applied to BFD. The load torque T_L can be described by [16]

$$T_L = T_0 + T_c \cos(\omega_c t), \text{ and } \omega_c = 2\pi f_c \quad (2)$$

where T_0 is a constant component and T_c is the amplitude of the bearing fault-related torque variations. By applying the mechanical equation of the machine, the torque variations $T(t)$ affect the motor speed $w_r(t)$ as follows:

$$T(t) = T_m(t) - T_L(t) = J\frac{dw_r}{dt} \Leftrightarrow w_r(t) = \frac{1}{J}\int_t (T_m(\tau) - T_L(\tau))d\tau \quad (3)$$

where T_m is the electromagnetic torque produced by the machine and J is the total inertia of the system machine load.

In steady state, the motor torque is assumed to be equal to the constant part of the load torque $T_m = T_0$, which leads to

$$w_r(t) = \frac{1}{J}\int_{t_0}^{t} -T_c \cos(\omega_c \tau)d\tau + C = \frac{-T_c}{J\omega_c}\sin(\omega_c t) + w_{r_0}. \quad (4)$$

Thus, theoretically, the rotor speed under bearing faults (ORF, IRF, and BBF) consists of a constant component w_{r_0} and a sinusoidally varying component.

The experimental rotor speed signal under the different bearing faults is shown in Fig. 2, which shows that this effect can be approximated by a sinusoidal form plus a noise component. Thus, a mathematical development of (4) is considered as follows.

From (2) and (4), the rotor speed yields

$$w_r(t) = \frac{-T_c}{2J\pi f_c}\sin(2\pi f_c t) + \eta + w_{r_0} \quad (5)$$

where η is white noise with zero mean and infinite variance. By considering f_{out}, f_{in}, and f_{ball} given by (1) in the bearing fault

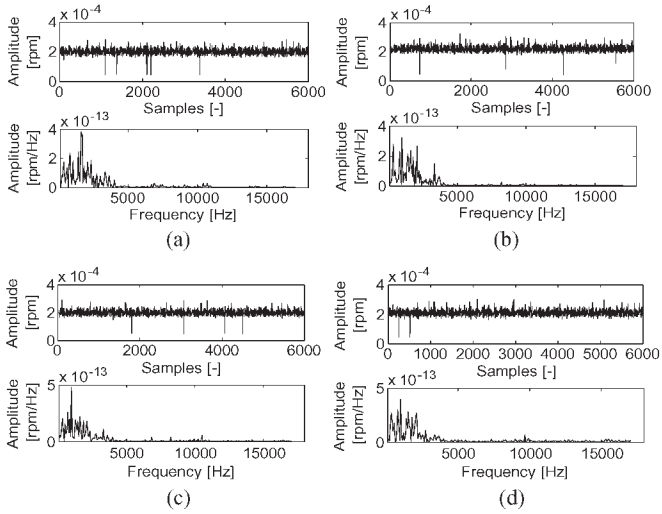

Fig. 3. Rotor speed signal in the time and frequency domains under (a) healthy and (b), (c), and (d) different bearing fault conditions.

cases, the rotor speed $w_r(t)$ becomes

$$\begin{cases} w_{r,out}(t) = \frac{-T_c}{J\pi D_{out}} \sin(\pi D_{out} t) + \eta + w_{r_0} & \text{for ORF} \\ w_{r,in}(t) = \frac{-T_c}{J\pi D_{in}} \sin(\pi D_{in} t) + \eta + w_{r_0} & \text{for IRF} \\ w_{r,ball}(t) = \frac{-T_c}{J\pi D_{ball}} \sin(\pi D_{ball} t) + \eta + w_{r_0} & \text{for BBF} \end{cases} \tag{6}$$

where the D's are defined by

$$D_{out} = \frac{N_b f_r (d_p - d_b \cos(\beta))}{d_p}; \quad D_{in} = \frac{N_b f_r (d_p + d_b \cos(\beta))}{d_p}$$

$$D_{ball} = \frac{f_r \left(d_p^2 - d_b^2 \cos(\beta)^2\right)}{d_p d_b}. \tag{7}$$

Equation (6) shows that the bearing faults' effect on the speed signal can be approximated by a sinusoidal form, which depends on the bearing geometry d_p, d_b, N_b, and the contact angle β with a noisy component η.

III. Proposed AVPCA for BFD

Although the use of rotor speed signals offers various benefits as discussed in the introduction, it is important to note that frequency domain analysis of the speed signal may be ineffective. Fig. 3 shows the time-domain experimental results of the speed signal under healthy and faulty bearing conditions and their power spectral density frequency response. Analyzing the frequency domain results shows that the effect of different bearing faults on the rotor speed signal is extremely similar even in the normal situation. Thus, frequency domain methods for BFD that are based on rotor speed signal are not wise choices. Instead, feature extraction methods [18]–[22], such as PCA, are preferable because the features of the speed signal under different healthy conditions exhibit different patterns.

PCA has been widely used as a tool to detect and diagnose faults [23]–[31]. However, classical PCA-based fault detection and diagnosis methods suffer from several drawbacks. First, the detection index is sensitive to the measurement data (presence or absence of noise and/or disturbances). Second, classical PCA cannot detect and/or diagnose the fault properly in a dependent failure case [23]. To overcome this problem, several researchers have proposed robust PCA methods [26]. However, researchers have only focused on the detection index and covariance matrix and involved more complicated mathematical changes.

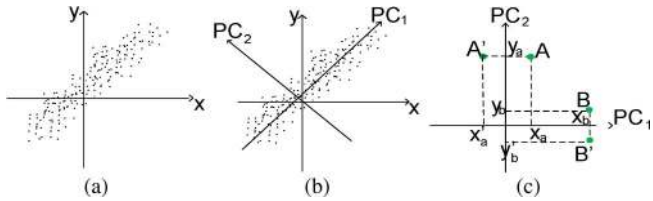

Fig. 4. Plot of random data: (a) random data in 2D; (b) projected random data to PCA subspace in PC1 and PC2; and (c) training data set − A and B; and testing data set −A′ and B′ in PCA subspace.

In this paper, to make PCA more appropriate for online BFD with no mathematical complication, we propose AVPCA, where the classical PCA is improved by calculating the PCA bases using the absolute value of the weights and sum of squared error (SSE) distances. Considering the SSE distance between the training PCA base and the test base, the fault can be assigned to a class under the released hypothesis of the minimum of the total SSE distance. Consider the example given in Fig. 4(a), where random data in 2D are supposed. Two retained principal components, PC_1 and PC_2, are used to project the data to the PCA subspace, as shown in Fig. 4(b). Let $\mathrm{A}\,(x_a,\ y_a)$ and $\mathrm{B}\,(x_b,\ y_b)$ be two data sets from the training set that belongs to class 1, and let $\mathrm{A}'\,(x'_a, y'_a)$ and $\mathrm{B}'\,(x'_b, y'_b)$ be two data sets from the same class 1 but obtained from new unknown data from the test set.

From trial observations and after analyzing different sets of measurements, as shown in Fig. 4(c), A′ and B′ will have the following coordinates:

$$\begin{cases} x'_a = -x_a \pm \varepsilon \\ y'_a = y_a \pm \varepsilon \end{cases} \quad \text{and} \quad \begin{cases} x'_b = x_b \pm \varepsilon \\ y'_b = -y_b \pm \varepsilon. \end{cases} \tag{8}$$

Computing the SSE distance ξ between these two values gives

$$\begin{cases} \xi_{x_a} = \|x'_a - x_a\|^2 = \|-x_a \pm \varepsilon - x_a\|^2 = \|-2x_a \pm \varepsilon\|^2 = (2x_a \pm \varepsilon)^2 \\ \xi_{y_a} = \|y'_a - y_a\|^2 = \|y_a \pm \varepsilon - y_a\|^2 = \|\pm\varepsilon\|^2 = \varepsilon^2 \\ \xi_{x_b} = \|x'_b - x_b\|^2 = \|x_b \pm \varepsilon - x_b\|^2 = \|\pm\varepsilon\|^2 = \varepsilon^2 \\ \xi_{y_b} = \|y'_b - y_b\|^2 = \|-y_b \pm \varepsilon - y_b\|^2 = \|-2y_b \pm \varepsilon\|^2 = (2y_b \pm \varepsilon)^2 \end{cases}$$

and the total SSE distance Ξ will be

$$\begin{cases} \Xi_A = \xi_{x_a} + \xi_{y_a} = (2x_a \pm \varepsilon)^2 + \varepsilon^2 \gg \varepsilon \\ \Xi_B = \xi_{x_b} + \xi_{y_b} = \varepsilon^2 + (2y_b \pm \varepsilon)^2 \gg \varepsilon. \end{cases} \tag{9}$$

Thus, the total SSE distance is magnified instead of minimized, which occurs when classical PCA is used. To address this situation, the absolute value of the bases is used in calculating the SSE distance, as shown below:

$$\begin{cases} \xi_{x_a} = \|abs(x'_a) - abs(x_a)\|^2 = \|abs(-x_a \pm \varepsilon) - abs(x_a)\|^2 = \varepsilon^2 \\ \xi_{y_a} = \|abs(y'_a) - abs(y_a)\|^2 = \|abs(y_a \pm \varepsilon) - abs(y_a)\|^2 = \varepsilon^2 \\ \xi_{x_b} = \|abs(x'_b) - abs(x_b)\|^2 = \|abs(x_b \pm \varepsilon) - abs(x_b)\|^2 = \varepsilon^2 \\ \xi_{y_b} = \|abs(y'_b) - abs(y_b)\|^2 = \|abs(-y_b \pm \varepsilon) - abs(y_b)\|^2 = \varepsilon^2. \end{cases}$$

TABLE I
OFFLINE TRAINING PROCEDURE STEPS BASED ON AVPCA

Step 1. Obtain a sample of the n output data from the rotor speed signal at instant k for both the fault-free case and the abnormal cases. The training vectors $W_{r_j}{}^m(k)$ will be defined by

$$W_{r_j}{}^m(k) = \left[w_{r_1}{}^m(k), w_{r_2}{}^m(k), \cdots, w_{r_n}{}^m(k) \right]^T, \tag{11}$$

where m is the number of all possible faulty cases and the fault-free case, which are known as clusters. In our application, $m=1$ for the BFF cluster, $m=2$ for the ORF cluster, $m=3$ for the IRF cluster, and $m=4$ for the BBF cluster. And $j=1,\ldots,n$, where n is the number of output rotor speed samples.

Step 2. Calculate the mean vector μ^m of each training vector and its orthogonal; then compute the orthonormal data vectors:

$$O_r{}^m(k) = orth\left(W_{r_j}{}^m(k) - \mu^m \right). \tag{12}$$

Step 3. Compute the normalized covariance matrix $C_{nor}{}^m$ for the orthonormal training data vectors:

$$C_{nor}^m = \frac{1}{n}\left(O_r{}^m(k) \cdot O_r{}^m(k)^T \right). \tag{13}$$

Step 4. Compute the eigenvalues λ_j^m and eigenvectors Φ_j^m of the normalized covariance matrix $C_{nor}{}^m$ and then arrange them in order from largest to smallest.

Step 5. Select the number of eigenvectors p based on the cumulative percent of variance (CPV) approach with a precision of CPV (p) ≥ 99.9% defined by

$$CPV(p) = 100 \cdot \sum_{i=1}^{p} \lambda_i \Big/ \sum_{i=1}^{n} \lambda_i. \tag{14}$$

The p retained Principal Components (PCs) are uncorrelated and arranged in decreasing variance order. These p retained eigenvectors Φ_i^m associate with the largest eigenvalues λ_i^m of the original data matrix $W_{r,\,[n\times m]}$ defines the principal component subspace $W_{r_{pc}}$ that represent the correct direction of the measured vectors, and the remaining n-p eigenvectors represent the direction of the faulty measurements, the residual subspace E, which is defined by

$$W_r = W_{r_{pc}} + E;\ W_{r_{pc}} = \hat{D}\hat{H}^T;\ \text{and}\ E = \tilde{D}\tilde{H}^T, \tag{15}$$

where $\hat{H}_{[m,p]}$ is the weight matrix defined by

$$\hat{H} = [h_1^m, h_2^m, \cdots, h_p^m]^T;\ i = 1, \cdots, p;\ p <<< n, \tag{16}$$

and $\hat{D}_{[m,p]}$ is the score matrix that should verify

$$\hat{D}_{[n,p]} = W_{r_{pc}} \hat{H}. \tag{17}$$

Step 6. Compute the absolute value of the weights

$$\chi_i^m = \left| h_i^m \right|, i = 1, \cdots, p. \tag{18}$$

Hence, the residual weights r_{h_i} will be defined by

$$r_{h_i} = \chi_i^m - \chi_{i\_q}^m, \tag{19}$$

where $\chi^m{}_{i\ q}$ is the weight vector describing the q^{th} database.

Step 7. Generate the PCA training database matrix

$$M_b^m = \left[\chi_1^m, \chi_2^m, \cdots, \chi_p^m \right]. \tag{20}$$

The total SSE will be

$$\begin{cases} \Xi_A = \xi_{x_a} + \xi_{y_a} = \varepsilon^2 + \varepsilon^2 = 2\varepsilon^2 \ll \varepsilon \\ \Xi_B = \xi_{x_b} + \xi_{y_b} = \varepsilon^2 + \varepsilon^2 = 2\varepsilon^2 \ll \varepsilon. \end{cases} \tag{10}$$

Equation (10) indicates that, by using the absolute value in the PCA, the total SSE distances are always minimized regardless of the bases signs. Rotor speed-based BFD using the proposed AVPCA is described in the following section.

IV. PROPOSED RSB-BFD USING AVPCA

The presence of bearing faults influences characteristic parameters, which causes the parameters to vary. A sample formed with the variations of the faulty parameters will contain specific information related to the fault itself. AVPCA extracts a number of characteristic vectors from these samples that are mutually orthogonal. To develop the AVPCA model for BFD, the study is divided into two procedures: 1) an offline training procedure; and 2) an online fault detection and diagnosis procedure. Hence, the collected speed signal data set is divided into two parts: training data (known data) and testing data (unknown data). The training data are regarded as the historic data and used to build the training database, whereas the testing data are used to verify the performance of the proposed RSB-BFD.

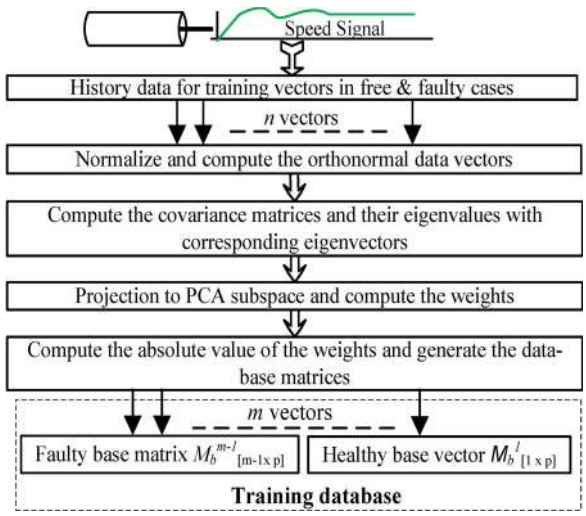

Fig. 5. Overview of the offline training procedure based on AVPCA.

TABLE II
ONLINE FAULT DETECTION AND DIAGNOSIS PROCEDURE

Step 8. A new set of data, called the data test vector $W_r^{new}(k)$, is projected onto the AVPCA subspace following the previous steps 1 to 6.

Step 9. Generate their AVPCA test database matrix

$$M_b^{new} = \left[\chi_1^{new}, \chi_2^{new}, \cdots, \chi_p^{new} \right]. \tag{21}$$

Step 10. Compute the SSE as

$$\xi^m = \left\| M_b^{new} - M_b^m \right\|^2. \tag{22}$$

A. Offline Training Procedure

Table I describes the offline training procedure, which contains the AVPCA steps.

The overall offline training procedure of the proposed AVPCA is summarized in Fig. 5.

B. Online Fault Detection and Diagnosis Procedure

After the offline training of the system in both healthy and faulty cases, the algorithm is ready for the online fault detection and diagnosis procedure, which is composed of the steps described in Table II.

The total SSE is given by $\Xi = \xi_1 + \xi_2 + \cdots + \xi_n$, which will be minimized at each stage of the cluster analysis. Considering a predefined threshold ρ, the fault can be detected. The overall online fault detection and diagnosis procedure for the proposed RSB-BFD is summarized in Fig. 6.

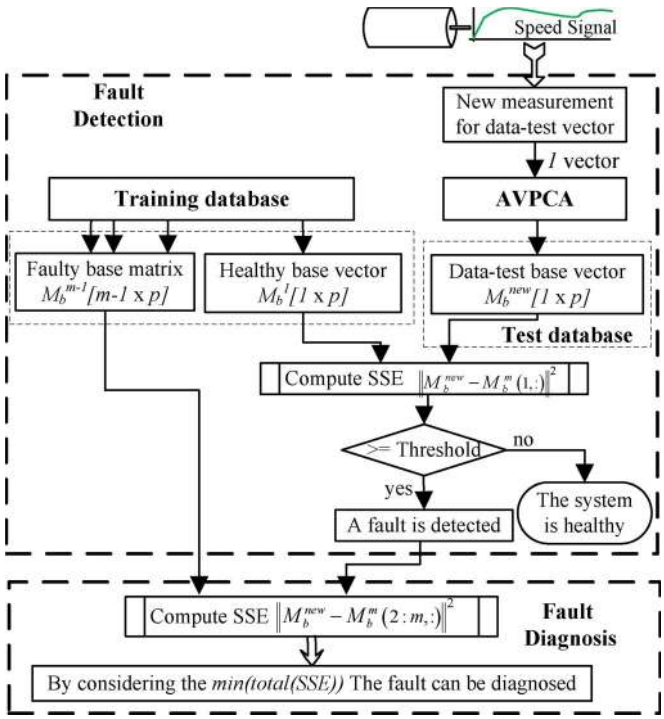

Fig. 6. Overview of the proposed online procedure for RSB-BFD.

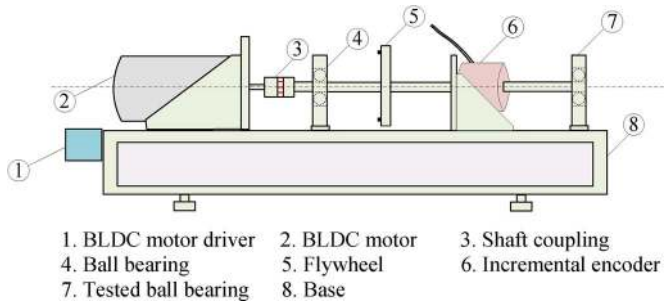

Fig. 7. Schematic diagram of the experimental setup.

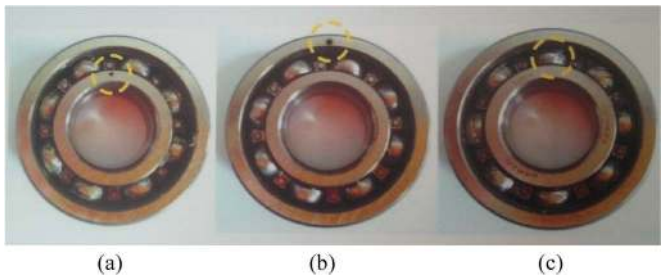

Fig. 8. Faulty ball bearings with a single hole: (a) IRF; (b) ORF; and (c) BBF.

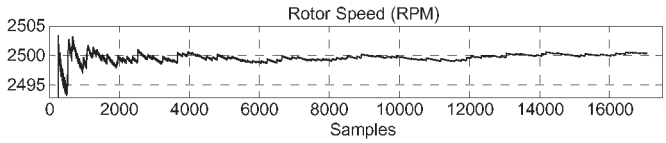

Fig. 9. Rotor speed signal from the incremental encoder output under a constant-speed environment.

Once the new test data set has been projected onto the AVPCA subspace, the fault has been detected. The fault diagnosis procedure is then used to diagnose a detected fault by projecting the new set of the test data into the subspaces spanned by the principal component vectors of the training set. If the similarity between the set and subspace is greater than the similarity with any other class, then the membership of the new set in a class can be determined using the SSE distance because this distance can achieve better extraction results with less training compared with other distances [32]. The fault is assigned to a class under the given hypothesis of the minimum distance SSE, which is used as a basis for testing and further investigation of the fault diagnosis task.

V. Experimental Results And Discussion

A. Experimental Setup

To evaluate the performance of the proposed RSB-BFD method, an experimental setup was built with a 750-W brushless direct current (BLDC) motor powered by a TMC-7 BLDC motor driver. The rotor speed was the only quantity measured. The schematic diagram of the experimental setup is illustrated in Fig. 7. Two ball bearings (NSK 6204) with eight balls were integrated in the experimental setup. The tested ball bearings were artificially damaged to produce flaws on the outer race, inner race, or ball. The flaws consisted of 1-mm holes that were drilled axially through the outer and inner raceways and the ball (see Figs. 1 and 8). A flywheel was added to the experimental setup to generate a constant load torque. All measured quantities were collected with a national instruments (NI) cDAQ-9178 eight-slot universal serial bus (USB) chassis. The NI9411 module was used for the rotor speed signal. The measured data were sampled at 17.06 kHz and processed using MATLAB R2012a.

The rotor speed signal for the proposed algorithm was measured with an incremental encoder type E60H NPN open collector output at 1024 pulses per revolution with a maximum allowable revolution of 6000 r/min.

Two different environments were considered: 1) constant-speed environment; and 2) variable-speed environment. First, a constant motor speed of $w_r = 2500$ r/min was considered while the bearing fault detection and diagnosis algorithm was running, as shown in Fig. 9.

B. Offline Training Procedure

For the offline training procedure, a set of historical process data from the motor rotor speed signal under different faulty bearing conditions (ORF, IRF, and BBF) and the healthy condition (BFF) was first measured and sampled to form the training data vectors $W_{r_j}^m(k)$ given by (11).

The SCREE [33] plot indicates that the number of PCs can be chosen as one $(p = 1)$. Using the CPV approach to obtain a precision of 99.9%, the number of principal components is fixed at three $(p = 3)$, as shown in Table III. The AVPCA projection reduces the original n-space to a 3-D subsystem in p-space.

Fig. 10 shows the variation of the residual weights r_{h_i} of the AVPCA subspace in 3-space for the healthy case and the three

TABLE III
CPV PRECISION OF THE EIGENVALUES

PC number	1	2	3
Eigenvalues	$3.74*10^{3}$	$3.63*10^{-12}$	$3.49*10^{-12}$
CPV[%]	99.7803	99.8475	99.8983

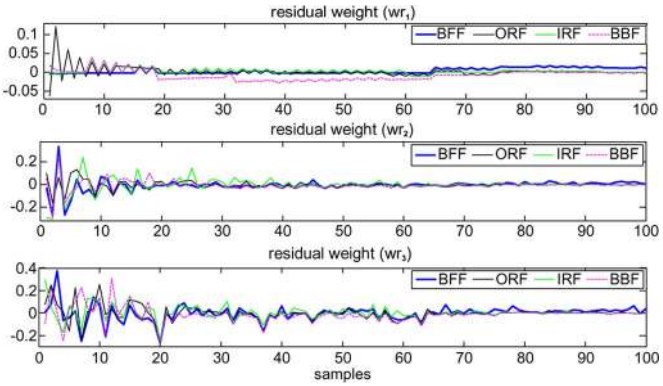

Fig. 10. Variation of residual weights.

TABLE IV
SUMMARY OF TOTAL SSE UNDER CONSTANT SPEED

		Total SSE distance to BFD			
		1	2	3	4
Training databases in the different bearing conditions	BFF	**0.00488**	0.01393	0.01231	0.03034
	ORF	0.00910	**0.00603**	0.01751	0.03885
	IRF	0.01096	0.01374	**0.01137**	0.03953
	BBF	0.01010	0.01340	0.01222	**0.02460**

faulty cases (ORF, IRF, and BBF). It is clear that BBFs cannot be detected using only the residual weights.

C. Online Fault Detection and Diagnosis Results Under Constant Speed

After performing the training procedure in the healthy and faulty cases, a new set of measurements from the rotor speed signal was considered to form the data test vector $W_r^{new}(k)$ that contains the unknown rotor speed signal measurements. Faults can thus be detected by evaluating the SSE distance between the data test vector and training vectors, as described in (22). By evaluating the SSE distance variation, computing the total SSE, and considering its minimum, the fault was detected and then diagnosed. The results of the total SSE distance with the proposed AVPCA for RSB-BFD at a constant-speed condition are summarized in Table IV.

D. Online Fault Detection and Diagnosis Results Under Variable Speed

Bearing fault detection and diagnosis under variable speed is more challenging though more realistic. Thus, as shown in Fig. 11, four scenarios with different profiles of variable motor speed w_r were considered while the RSB-BFD algorithm was running.

Fig. 11 shows the variation of the SSE distance between the unknown data test vector $W_r^{new}(k)$ on the nonfaulty case and the training vectors $W_r^m(k)$ (where $m = 1, 2, 3, 4,$) using

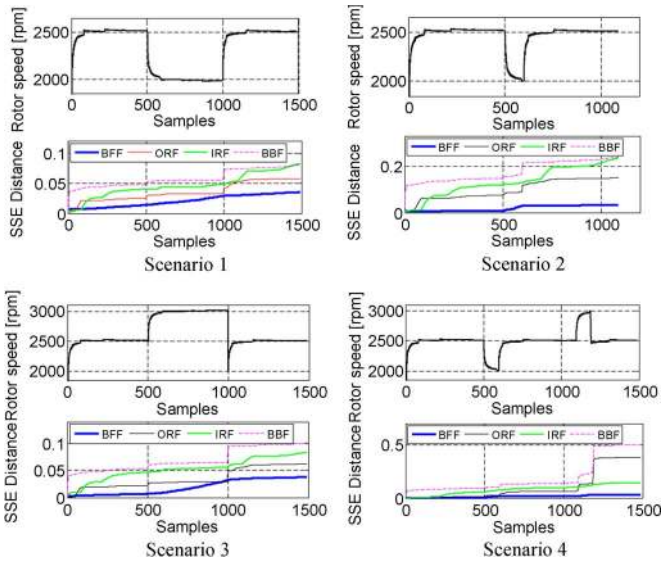

Fig. 11. SSE distance calculated by AVPCA under variable speed with four scenarios.

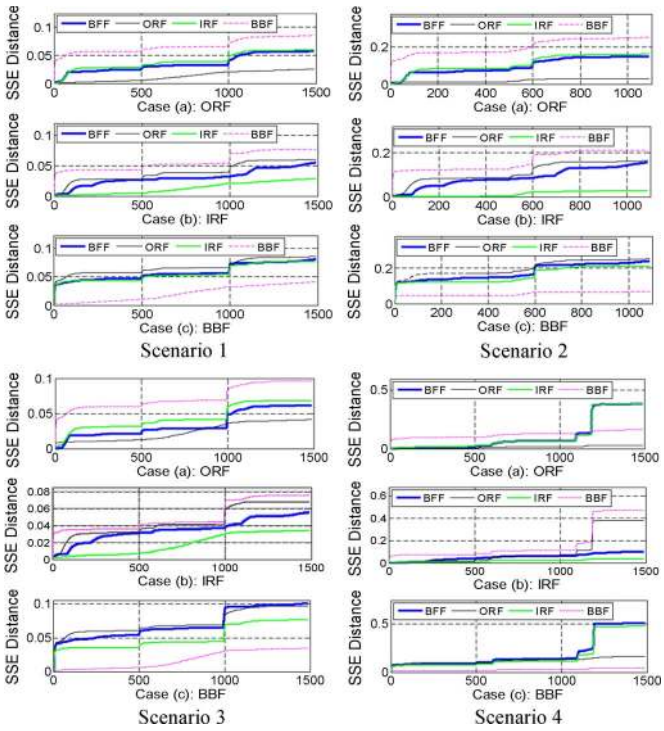

Fig. 12. SSE distance calculated by AVPCA for BFD under variable speed with four scenarios.

the proposed AVPCA as the RSB-BFD fault detection method under the four scenarios with different speed profiles and fault cases. In this figure, the SSE distance for the proposed AVPCA can clearly be used to detect any of the faults in all of the measurement sets. The SSE distance variation in the BFF case was always less than the SSE distance variation for all the fault cases (ORF, IRF, and BBF).

Fig. 12 and Table V depict respectively the SSE distance variation and the total SSE distance in tested cases (2), (3), and (4) by the proposed RSB-BFD for fault diagnosis. Fig. 12 shows

TABLE V
SUMMARY OF TOTAL SSE UNDER VARIABLE SPEED

			Total SSE distance for bearing fault detection and diagnosis								
		Tested-cases / Trained-cases	(1)	(2)	(3)	(4)		Tested-cases / Trained-cases	(1)	(2)	(3)	(4)
Training databases in the different healthy bearing conditions	Scenario. 1	BFF	**0.035**	0.057	0.055	0.080	Scenario.3	BFF	**0.037**	0.062	0.055	0.101
		ORF	0.057	**0.025**	0.060	0.085		ORF	0.062	**0.041**	0.068	0.096
		IRF	0.082	0.060	**0.028**	0.076		IRF	0.083	0.068	**0.034**	0.075
		BBF	0.080	0.085	0.076	**0.041**		BBF	0.101	0.096	0.075	**0.034**
	Scenario. 2	BFF	**0.032**	0.149	0.157	0.24	Scenario.4	BFF	**0.031**	0.382	0.096	0.503
		ORF	0.149	**0.03**	0.163	0.253		ORF	0.382	**0.028**	0.383	0.161
		IRF	0.235	0.163	**0.027**	0.211		IRF	0.145	0.383	**0.036**	0.473
		BBF	0.24	0.253	0.211	**0.068**		BBF	0.503	0.161	0.473	**0.042**

the SSE distance calculated by AVPCA for BFD for the four different scenarios. It can be seen that, in each scenario, the minimum in case a): ORF is the black line that represents the evaluation of the SSE distance when the ORF was considered for the test data. The minimum in case b): IRF is the green line that represents the evaluation of the SSE distance when the IRF was considered for the test data. In addition, the minimum in case c): BBF is the magenta line that represents the evaluation of the SSE distance when the ball fault was considered for the test data. Thus, it is clear that the minimum of the SSE corresponds to the faulty case.

Furthermore, Table V shows the total SSE distance calculated by AVPCA for BFD under the four different scenarios. It can also be observed that, in each scenario, for the ORF case, the minimum of the total SSE is case (2), which corresponds exactly to the ORF case. For the IRF case, the minimum of the total SSE is case (3), which is equal to the IRF case. Similar results were obtained for the BBF case, where the minimum of the total SSE is case (4), which exactly corresponds to the ball fault case. Hence, the detected fault can be diagnosed in all four considered scenarios with different varying speed profiles.

Analysis of the SSE distance evaluation in Figs. 11 and 12 shows that the SSE evaluation generally increases during the transient part compared with that of the steady-state part. Therefore, the bearing fault has a greater effect on the rotor speed in the variable-speed environment than in the constant-speed environment.

E. Comparison of AVPCA and Classical PCA for RSB-BFD

The main drawback in applying the classical PCA algorithm for fault detection and diagnosis is the sensitivity of the PCA model to the measurement data and the dependence or independence of the measured data. Furthermore, it has been shown that PCA cannot satisfactorily perform detection if the number of data sets is large, whereas a PCA model constructed from a small number of data sets can successfully detect and diagnose a fault [34]. Unfortunately, in BFD applications, the system is highly noisy, and the number of data sets is very large due to the higher sampling rate (order of 10^{-5} s).

This section highlights the benefit of AVPCA over the classical PCA. The classical PCA and proposed AVPCA bases were performed on ten different sets of measurements for each of the fault and healthy cases under constant speed. In addition, under the variable-speed environment, each of the fault and healthy cases was tested with 20 different sets of measurements, where each fault case consisted of five measurement sets.

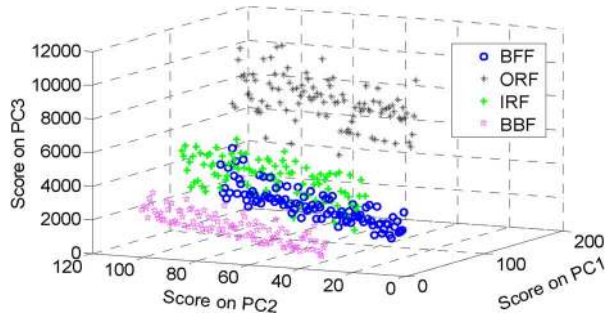

Fig. 13. PCA score plot of rotor speed under normal and fault conditions.

For the 30 different sets of measurements, the eigenvalue plot and the AVPCA score plot (see Fig. 13) from the analysis of the bearing experiments under normal and faulty conditions exhibit some overlap between the BFF, BBF, and IRF cases. This overlap in the eigenvalue clusters of healthy and different fault cases affects the effectiveness of the classical PCA for bearing fault detection and diagnosis.

Details of the comparison between AVPCA and the classical PCA under the constant-speed and variable-speed environments for BFD are presented in Fig. 14 with a summary in Table VI.

Case A. Constant-Speed Environment: The proposed AVPCA can detect the fault in nine measurement sets and fails in only one case (measurement set 5), whereas the classical PCA fails in three sets, which is due to the weight's sign variation. For additional clarity, let us consider measurement set 1 for both algorithms. The total SSE is equal to the square norm of the difference between the training database vectors M_b^m and the test database vectors M_b^{new}. In set 1, M_b^m is positive (let M_b^m be $+\mathrm{A}$), and the test database vector M_b^{new} is negative (let M_b^{new} be $-\mathrm{A} \pm \varepsilon$), i.e.,

$$\Xi = \|M_b^{new} - M_b^m\|^2 = \|-A \pm \varepsilon - A\|^2 = (2A \pm \varepsilon)^2 \quad \text{via Classical PCA} \tag{23a}$$

$$\Xi = \|M_b^{new} - M_b^m\|^2 = \|abs(-A \pm \varepsilon) - abs(A)\|^2 = \|\varepsilon\|^2 = \varepsilon^2 \quad \text{via AVPCA} \tag{23b}$$

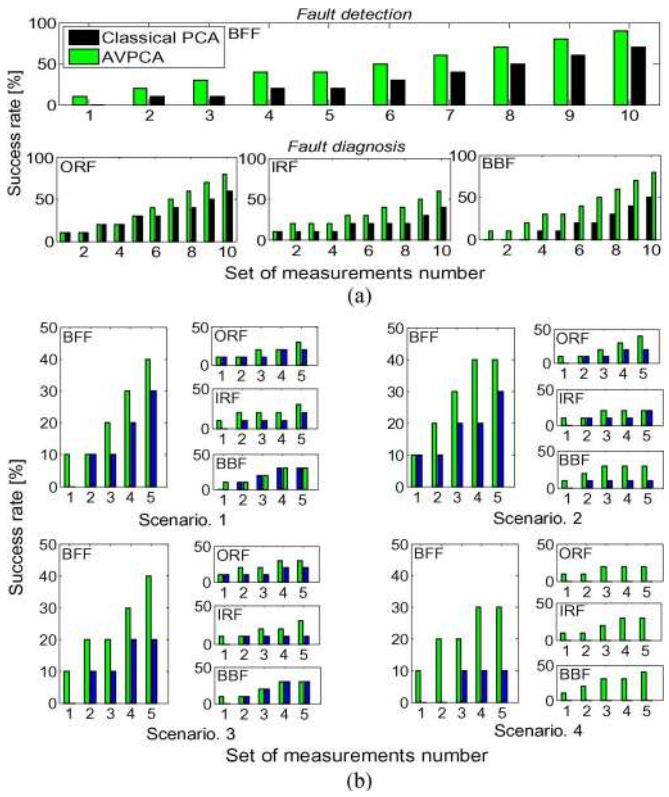

Fig. 14. Comparison of AVPCA and classical PCA for RSB-BFD in both constant and variable-speed environments in terms of *the success rate of fault detection and diagnosis*. (a) Constant-speed environment. (b) Variable-speed environment.

TABLE VI
SUMMARY OF RSB-BFD EFFICIENCY UNDER BOTH CONSTANT AND VARIABLE SPEED ENVIRONMENTS

		Constant speed				Variable speed			
Success rate [%]	Method \ Task	Fault detection	Fault diagnosis			Fault detection	Fault diagnosis		
Classical PCA		BFF	ORF	IRF	BBF	BFF	ORF	IRF	BBF
		70	60	40	50	**45**	30	20	35
			Average: **50**				Average:**28.3**		
AVPCA		BFF	ORF	IRF	BBF	BFF	ORF	IRF	BBF
		90	80	60	80	**75**	60	55	65
			Average: **73.3**				Average: **60**		

Thus, the total SSE is magnified instead of minimized via the classical PCA (23a). However, by considering the absolute value of the weights via the proposed AVPCA, the total SSE is always minimized regardless of the weight's sign (23b). This simple addition permits AVPCA to achieve the success rate (i.e., fault detection rate) of 90%, which is greater than the 70% success rate achieved with the classical PCA. A similar result was obtained for the fault diagnosis; the success rates with AVPCA and the classical PCA were 73.3% and 50%, respectively.

Case B. Variable-Speed Environment: In this case, an even more challenging though more realistic situation was considered using four different variable-speed scenarios. AVPCA was capable of detecting the bearing faults with a 75% success rate and could diagnose those faults with a 60% success rate in the 20 tests. In contrast, the classical PCA did not effectively detect the bearing faults (45%) and essentially could not diagnose the detected faults (28.3%), which is due to the overlap between the healthy bearing conditions (dependent faults) and the speed variation.

TABLE VII
SUMMARY OF BFD EFFICIENCY FOR ROTOR SPEED-BASED AND VIBRATION-BASED METHODS UNDER CONSTANT- AND VARIABLE-SPEED ENVIRONMENTS

		Constant speed				Variable speed			
Success rate [%]	Method \ Task	Fault detection	Fault diagnosis			Fault detection	Fault diagnosis		
Rotor speed-based		BFF	ORF	IRF	BBF	BFF	ORF	IRF	BBF
		90	80	60	80	**75**	60	55	65
			Average: **73.3**				Average: **60**		
Vibration-based		BFF	ORF	IRF	BBF	BFF	ORF	IRF	BBF
		92.5	85	70	75	**63.3**	55	40	45
			Average: **76.7**				Average: **46.7**		

F. Comparison of Rotor Speed-Based and Vibration-Based Methods Using AVPCA for BFD

To explore the advantage of the rotor speed-based approach over vibration-based BFD, the success rates under constant- and variable-speed environments are compared in Table VII. Both methods are implemented using the proposed AVPCA.

Table VII shows that a vibration-based method using AVPCA was capable of detecting the bearing faults with a 92.5% success rate and could diagnose those faults with a 76.7% success rate under constant-speed environment, which is slightly better than the proposed rotor speed-based method. However, under the variable-speed environment, the rotor speed-based method, which detected and diagnosed the bearing faults with a 75% and a 60% success rate, respectively, was able to achieve a significantly higher success rate than the vibration-based method. These results highlight the benefit of the proposed RSB-BFD using AVPCA under the varying speed environment where the vibration signal from the bearing is affected by operation, which makes diagnosis difficult. This difficulty results from the variation of diagnostic features caused primarily by speed variations, low energy of sought features, and high noise levels.

VI. CONCLUDING REMARKS

In this paper, a novel BFD method, the RSB-BFD, was proposed. Because the proposed method was only based on rotor speed signals, it is beneficial in terms of system cost and simplicity. To address the difficulty caused by the overlapping conditions, the classical PCA was modified to AVPCA, in which the PCA bases are evaluated using the absolute value of weights and SSE distances.

The proposed method was examined under both a constant-speed and a variable-speed environment, where the load remained constant. Three different bearing faults (ORF, IRF, and ball fault) were artificially introduced to demonstrate the performance of the proposed method. A set of experiments showed that the proposed RSB-BFD improved the fault detection and fault diagnosis performance by more than 20% in the

constant-speed case and by 30% in the variable-speed case. Comparative studies between AVPCA and the classical PCA and between the rotor speed-based and the vibration-based methods showed the effectiveness of the proposed method.

For future work, field tests will be conducted under real conditions including the influence of load variations, motor types, bearing types, and initial conditions. To make the proposed algorithm more adequate in real environment, it is also necessary to improve the ability of distinguishing the fault from other sources of speed oscillation.

References

[1] S. Choi, B. Akin, M. Rahimian, and H. Toliyat, "Performance-oriented electric motors diagnostics in modern energy conversion systems," *IEEE Trans. Ind. Electron.*, vol. 59, no. 2, pp. 1266–1277, Feb. 2012.

[2] IEEE Motor Reliability Working Group, "Report of large motor reliability survey of industrial and commercial installations," *IEEE Trans. Ind. Appl.*, vol. IA-21, no. 4, pp. 853–872, Jul. 1985.

[3] C. Bianchini, F. Immovilli, M. Cocconcelli, R. Rubini, and A. Bellini, "Fault detection of linear bearings in brushless ac linear motors by vibration analysis," *IEEE Trans. Ind. Electron.*, vol. 58, no. 5, pp. 1684–1694, May 2011.

[4] W. Zhou, T. G. Habetler, and R. G. Harley, "Bearing condition monitoring methods for electrical machines: A general review," in *Proc. IEEE SPEEDAM*, Cracow, Poland, Sep. 6–8, 2007, pp. 3–6, CD-ROM Paper.

[5] V. Venkatasubramanian, R. Rengaswamy, S. N. Kavuri, and K. Yin, "A review of process fault detection and diagnosis Part III: Process history based methods," *Comput. Chem. Eng.*, vol. 27, no. 3, pp. 327–346, Mar. 2003.

[6] S. Nandi and H. A. Toliyat, "Condition monitoring and fault diagnosis of electrical machines: A review," *IEEE Trans. Energy Convers.*, vol. 20, no. 4, pp. 719–729, Dec. 2005.

[7] C. A. Walford, "Wind turbine reliability: Understanding and minimizing wind turbine operation and maintenance costs," Sandia Nat. Lab., Albuquerque, NM, USA, Rep. SAND2006-1100, Mar. 2006.

[8] B. Lu, Y. Li, X. Wu, and Z. Yang, "A review of recent advances in wind turbine condition monitoring and fault diagnosis," in *Proc. PEMWA*, 2009, pp. 1–7.

[9] C. J. Crabtree, "Survey of commercially available condition monitoring systems for wind turbines," School Eng. Comput. Sci., Durham Univ., Durham, U.K., Nov. 2010, Revision: 05.

[10] S. Sheng and P. Veers, "Wind turbine drivetrain condition monitoring-An overview," presented at the Mechanical Failures Prevention Group: Applied Systems Health Management Conf.Virginia Beach, VA, USA, May 10–12, 2011, Paper NREL/CP-5000-50698.

[11] F. Immovilli, C. Bianchini, M. Cocconcelli, A. Bellini, and R. Rubini, "Bearing fault model for induction motor with externally induced vibration," *IEEE Trans. Ind. Electron.*, vol. 60, no. 8, pp. 3408–3418, Aug. 2013.

[12] H. Zhang *et al.*, "Research on rolling bearing fault diagnosis with adaptive frequency selection based on LabVIEW," *Int. J. Control Autom.*, vol. 7, no. 3, pp. 93–100, Mar. 2014.

[13] J. Dybała and R. Zimroz, "Rolling bearing diagnosing method based on empirical mode decomposition of machine vibration signal," *Appl. Acoust.*, vol. 77, pp. 195–203, 2014.

[14] K. Javed, R. Gouriveau, N. Zerhouni, and P. Nectoux, "Enabling health monitoring approach based on vibration data for accurate prognostics," *IEEE Trans. Ind. Electron.*, vol. 62, no. 1, pp. 647–656, Jan. 2015.

[15] X. Gong and W. Qiao, "Bearing fault diagnosis for direct-drive wind turbines via current-demodulated signals" *IEEE Trans. Ind. Electron.*, vol. 60, no. 8, pp. 3419–3428, Aug. 2013.

[16] M. Blodt, P. Granjon, B. Raison, and G. Rostaing, "Models for bearing damage detection in induction motors using stator current monitoring," *IEEE Trans. Ind. Electron.*, vol. 55, no. 4, pp. 1813–1822, Apr. 2008.

[17] J. R. Stack, T. G. Habetler, and R. G. Harley, "Fault classification and fault signature production for rolling element bearings in electric machines," *IEEE Trans. Ind. Appl.*, vol. 40, no. 3, pp. 735–739, May/Jun. 2004.

[18] F. Jiang, Z. Zhu, W. Li, G. Chen, and G. Zhou, "Robust condition monitoring and fault diagnosis of rolling element bearings using improved EEMD and statistical features," *Meas. Sci. Technol.*, vol. 25, no. 2, pp. 1–14, 2014.

[19] L. Zhao, W. Yu, and R. Yan, "Rolling bearing fault diagnosis based on CEEMD and time series modeling," *Math. Probl. Eng.*, vol. 2014, 2014, Art. ID. 101867.

[20] H. Liu, X. Wang, and C. Lu, "Rolling bearing fault diagnosis under variable conditions using Hilbert-Huang transform and singular value decomposition," *Math. Probl. Eng.*, vol. 2014, 2014, Art. ID. 765621.

[21] T. W. Rauber, F. de Assis Boldt, and F. M. Varejão, "Heterogeneous feature models and feature selection applied to bearing fault diagnosis," *IEEE Trans. Ind. Electron.*, vol. 62, no. 1, pp. 637–646, Jan. 2015.

[22] M. Amar, I. Gondal, and C. Wilson, "Vibration spectrum imaging: A novel bearing fault classification approach," *IEEE Trans. Ind. Electron.*, vol. 62, no. 1, pp. 494–502, Jan. 2015.

[23] M. F. Harkat, G. Mourot, and J. Ragot, "An improved PCA scheme for sensor. FDI: Application to an air quality monitoring network," *J. Process Control*, vol. 16, no. 6, pp. 625–634, Jul. 2006.

[24] C. F. Alcala and S. J. Qin, "Reconstruction based contribution for process monitoring," *Automatica*, vol. 45, no. 7, pp. 1593–1600, Jul. 2009.

[25] A. benaicha, M. Guerfel, N. Bouguila, and K. benothman, "New PCA-based methodology for sensor fault detection and localization," presented at the *8th Int. Conf. Modeling Simul.*, Hammamet, Tunisia, May 10–12, 2010.

[26] Y. Tharrault, G. Mourot, J. Ragot, and D. Maquin, "Sensor fault detection and isolation by robust principal component analysis," in *Fault Detection*, W. Zhang, Ed. Rijeka, Croatia: In-Tech, chap. 16, 2010.

[27] Q. Jiang, X. Yan, and W. Zhao, "Fault detection and diagnosis in chemical processes using sensitive principal component analysis," *Ind. Eng. Chem. Res.*, vol. 52, no. 4, pp. 1635–1644, 2013.

[28] B. Wang, Q. Jiang, and X. Yan, "Fault detection and identification using a Kullback-Leibler divergence based multi-block principal component analysis and Bayesian inference," *Korean J. Chem. Eng.*, vol. 31, no. 6, pp. 930–943, Jun. 2014.

[29] J. Harmouche, C. Delpha, and D. Diallo, "Incipient fault detection and diagnosis based on Kullback-Leibler divergence using principal component analysis: Part I," *Signal Process.*, vol. 94, pp. 278–287, Jan. 2014.

[30] J. Harmouche, C. Delpha, and D. Diallo, "Incipient fault detection and diagnosis based on Kullback-Leibler divergence using principal component analysis: Part II," *Signal Process.*, vol. 109, pp. 334–344, Apr. 2015.

[31] D. You, X. Gao, and S. Katayama, "WPD-PCA-based laser welding process monitoring and defects diagnosis by using FNN and SVM," *IEEE Trans. Ind. Electron.*, vol. 62, no. 1, pp. 628–636, Jan. 2015.

[32] V. Perlibakas, "Distance measures for PCA-based face recognition," *Pattern Recog. Lett.*, vol. 25, no. 6, pp. 711–724, Apr. 2004.

[33] R. B. Cattell, "The SCREE test for the number of factors," *Multivariate Behav. Res.*, vol. 1, no. 2, pp. 245–276, 1966.

[34] J. Yu, "Local and nonlocal preserving projection for bearing defect classification and performance assessment," *IEEE Trans. Ind. Electron.*, vol. 59, no. 5, pp. 2363–2376, May 2012.

Moussa Hamadache (S'15) received the State Engineering degree in automation of industrial processes from the University of M'hamed Bougara Boumerdes, Boumerdes, Algeria, in 2008. Since September 2009, he has been working toward the Ph.D. degree at the School of Electronics Engineering, Kyungpook National University, Daegu, Korea.

His research interests include statistical process monitoring, model-based and data-driven-based fault detection and diagnosis techniques in rotating electrical machinery, filtering, and control engineering.

Dongik Lee (M'15) received the B.S. and M.S. degrees in control engineering from Kyungpook National University, Daegu, Korea, in 1987 and 1990, respectively, and the Ph.D degree in complex systems control engineering from Sheffield University, Sheffield, U.K., in 2002.

He is currently an Associate Professor of the School of Electronics Engineering, Kyungpook National University. His research interest focuses on the design of real-time networked control for various safety-critical applications, including autonomous underwater vehicles, wind turbines, and intelligent automobiles.

Kalyana C. Veluvolu (S'03–M'06–SM'13) received the B.Tech. degree in electrical and electronic engineering from Acharya Nagarjuna University, Guntur, India, in 2002, and the Ph.D. degree in electrical engineering from Nanyang Technological University, Singapore, in 2006.

During 2006–2009, he was a Research Fellow with the Biorobotics Group, Robotics Research Center, Nanyang Technological University. Since 2009, he has been with the School of Electronics Engineering, Kyungpook National University, Daegu, Korea, where he is currently an Associate Professor. He has been a Principal Investigator or a Coinvestigator on a number of research grants funded by the National Research Foundation of Korea, and other agencies. He has authored or coauthored over 100 journal articles and conference proceedings. His current research interests include nonlinear estimation and filtering, sliding mode control, brain–computer interface, biomedical signal processing, and surgical robotics.